9-15-1994

High Resolution Electron Beam Induced Current Measurements in an Scanning Tunneling Microscope on GaAs-MESFET

P. Koschinski
Bergische Universität Wuppertal

V. Dworak
Bergische Universität Wuppertal

L. J. Balk
Bergische Universität Wuppertal

Recommended Citation

Utah State University
MERRILL-CAZIER LIBRARY

HIGH RESOLUTION ELECTRON BEAM INDUCED CURRENT MEASUREMENTS IN AN SCANNING TUNNELING MICROSCOPE ON GaAs-MESFET

P. Koschinski, V. Dworak, and L. J. Balk[*]

Sonderforschungsbereich 254, Bergische Universität Wuppertal,
Lehrstuhl für Elektronik, Fuhlrottstr. 10, D-42097 Wuppertal

Abstract

Recently, the first results of electron beam induced current (EBIC) measurements in a scanning tunneling microscope (STM) have been reported. Although the acquired results match with those obtained in conventional EBIC investigations, the interpretation of the obtained results is still restricted solely to a qualitative discussion. In this paper, a quantitative approach is used for two-dimensional numerical simulations of induced currents in GaAs-MESFET leading to a first starting point for a sophisticated interpretation of the dependence of induced currents on experimental and device parameters.

Key words: Electron beam induced current, simulation, scanning tunneling microscope, MESFET.

[*]Address for correspondence:
Ludwig J. Balk
Sonderforschungsbereich 254,
Bergische Universität Gesamthochschule Wuppertal
Lehrstuhl fur Elektronik
Fuhlrottstraße 10,
D-42097 Wuppertal
Germany
Telephone number: (+49-202) 439 2972
FAX number: (+49-202) 439 3040

Introduction

Today, the scanning tunneling microscope (STM) is an established tool in material and device analysis. Since the STM, as all scanning probe microscopes, exhibits an extremely high spatial resolution and since STMs and scanning electron microscopes (SEMs) are alike in their basic arrangement, efforts were made to extend the application of STMs to the field of material and device analysis and characterization usually performed in SEMs. As a consequence, several SEM measurement techniques are successfully applied to STMs, too, e.g., STM-cathodoluminescence [6] or STM-electron beam induced current (STM-EBIC) measurements [3]. These transferred techniques use the tunneling tip as an electron source for primary electrons (PE) in the energy range of up to some ten electron volts. Ballistic electron emission microscopy (BEEM) measurements on metal-semiconductor contacts demonstrated that, if the energy of the PE is sufficiently high, an electron-hole-pair generation (e-h-pair generation) can occur [5]. A measurement of an electron beam induced current in devices is possible if the e-h pairs are generated, e.g., within the depletion region of a Schottky contact of a metal semiconductor field effect transistor. The first measurements of electron beam induced currents in an STM in GaAs-MESFET have already been reported [4]. The present paper confirms the obtained measurement results by numerical simulations of induced currents in GaAs-MESFET in STM-EBIC investigations. Furthermore a detailed description of the STM-EBIC specific interaction between the tunneling tip and the sample device is presented.

Calculation of Induced Currents in Devices

The induced current can be described, just as any other current through a semiconductor device, by the basic semiconductor equations, namely Poisson's equation:

$$\Delta\phi = -e/\varepsilon_S \, (p - n + N_D - N_A + C), \qquad (1)$$

and the continuity equations for electrons and holes,

$$\partial p/_{\partial t} = -1/_e \, \mathrm{div} \, \overrightarrow{J}_p + G_{ext} - GR \qquad (2)$$

and

$$\partial n/_{\partial t} = 1/_e \, \mathrm{div} \, \overrightarrow{J}_n + G_{ext} - GR. \qquad (3)$$

The current densities can be related to potential differences or charge density gradients by the drift-diffusion approximation:

$$\overrightarrow{J}_p = -e \cdot p \cdot \mu_p \cdot \mathrm{grad} \, \phi - e \cdot D_p \cdot \mathrm{grad} \, p \qquad (4)$$

$$\overrightarrow{J}_n = -e \cdot n \cdot \mu_n \cdot \mathrm{grad} \, \phi + e \cdot D_n \cdot \mathrm{grad} \, n. \qquad (5)$$

The term G_{ext} represents the generation of e-h pairs, i.e., their spatial distribution $\langle f(\overrightarrow{r}) \rangle$ and their generated number per second. The number generated per second can easily be determined by the ratio of required energy to form an e-h pair to the energy of the PE, thus leading to:

$$G_{ext} = \frac{W_{PE} \cdot I_{PE}}{W_{eh} \cdot e} \cdot \langle f(\overrightarrow{r}) \rangle. \qquad (6)$$

To quantitatively describe the spatial distribution of the generated e-h pairs within the semiconductor, knowledge of the behaviour of the primary electrons in the sample, i.e., their trajectories and their energy loss along these trajectories, is required. Although the knowledge of low energy electron (> 100 eV) behaviour in solids is growing [1], an applicable expression in terms of charge densities and energy dissipation functions in the electron volt range is not available. An approach originated in scattering spectroscopy using a description of the incident electron as a wave in phase space under the assumption of momentum conservation is developed [2] but not applicable to the formulas given above, since this description does not supply any information on the spatial distribution in real space.

Numerical Calculations of Induced Currents

The system of basic semiconductor equations can only be solved numerically due to the complex boundary conditions necessary for real devices. A program capable of solving this equation system by the finite differences method is the device simulator MINIMOS 5.1 (Inst. for Microelectronics, Tech. Univ., Vienna). This program allows two-dimensional, time independent simulations of field effect transistors. The simulation variables of this program are the electrostatical potential, the electron and the hole concentration. All other quantities,
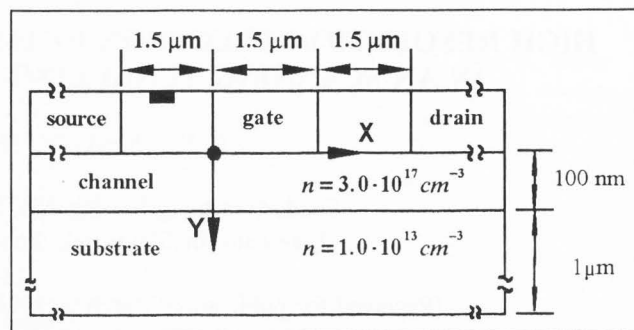

Figure 1. Cross-section of the simulated device.

----

e.g., the current densities or electrical field strengths are deduced from these basic parameters. In order to simulate induced currents, the program is modified. The modifications concern the continuity equation, where an additional term is required to take the external generation of e-h pairs into account, and the definition of the boundary conditions because the biased tunneling tip acts as an additional electrode. The details of the simulation are given below.

Simulation domain and boundary conditions

Figure 1 shows a cross-section, hereafter referred to as the simulation plane, of the simulated device. All subsequently presented quantities are calculated two-dimensionally in the simulation plane. The origin of the coordinate system of the simulation plane is located on the semiconductor surface at the left gate contact edge. The device is assumed to be homogeneous in the third dimension. The boundary condition for the electrostatic potential is determined by the applied voltages to the terminal contacts which are chosen to be zero volts at all terminal contacts. The tunneling tip with the applied voltage, acting as an additional flat electrode, is considered by introducing an appropriate boundary condition for the tip. The influence of the tip on the electrical properties in the simulation plane is calculated by solving Laplace's equation $= 0$ in the region above the semiconductor surface, assuming no charges are present.

Spatial distribution of the generated excess carriers

Since no applicable descriptions of the spatial distribution of the generated excess carriers are available, a homogeneous generation underneath the tip with a linear decay in depth and a maximum primary electron penetration depth of 20 nm is assumed. Figure 2 shows the generation rate, G_{ext}, for a tip position $x = -280$ nm from the left gate contact with a tip bias of ten volts, an emission current of 2 nA, and a tip width of 40 nm. A maximum generation rate of $1.7 \cdot 10^{17}$ cm^{-3} s^{-1} occurs at the semiconductor surface. Even though we believe
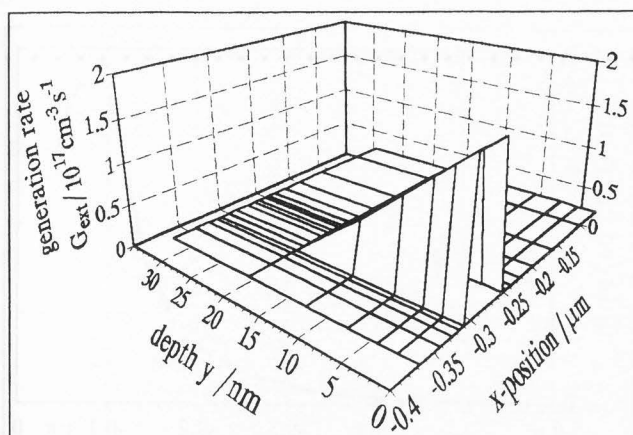
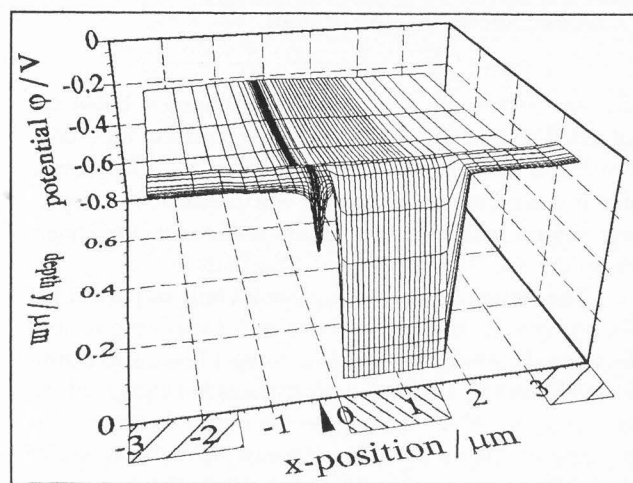**Figure 2.** Spatial distribution of the generation rate, G_{ext}.

Figure 3. Potential distribution in the simulation plane (arrow marks the tip position).

----

that the resulting induced current is not extremely sensitive to the shape of the generation volume the distribution function $\langle f(\overline{r}) \rangle$ should be adjusted to further results.

Simulation results

This section presents the calculated simulation quantities in the simulation plane. The simulation plane forms the base plane, and the calculated quantity is plotted along the third axis dependent on its value at a specific location in the simulation plane. Figure 3 shows the potential distribution in the simulation plane with the tunneling tip at the position x = -280 nm. The voltage applied to the tip is -10 V with an emission current of 2 nA. The potential drop of approximately 0.7 V under the Schottky contact is clearly visible. Beside this potential drop, an additional potential drop at the tip
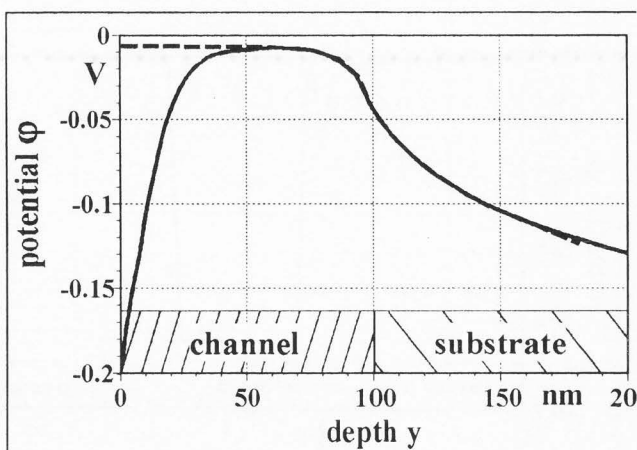

Figure 4. Depth dependence of the electrostatic potential (solid curve: with tunneling tip present, dashed curve: without tunneling tip).

----

position is present. This is the influence of the negatively biased tip on the potential distribution in the semiconductor region. Figure 4 shows the depth dependence of the electrostatic potential in the semiconductor for the same simulation parameters. The dashed curve represents the potential curvature of the undisturbed semiconductor without a tip. The potential drop at y = 100 nm is caused by the different doping levels of the semiconductor between the channel region and the substrate. The solid line represents the potential with a tip present. The biased tip causes a change of the potential up to a depth of 50 nm in the semiconductor. The biased tip has the same effect on the conducting channel of the device as the gate electrode, thus controlling the current through the device if the device terminals are biased. Since the tip behaves as an electrode, an MIS-like structure is given, and, consequently, the extent of the potential change in depth depends, e.g., on the applied voltage to the tip, on the doping level of the semiconductor, and on the presence of charged surface states. It should therefore be possible to use the field effect between the tip, without emitting any current, and the semiconductor as a probe for existing surface states. Besides this influence, the tip changes the spatial dependence of the potential in the lateral direction as well. Figure 5 indicates the lateral variation of the potential at the semiconductor surface in the vicinity of the tip. The extent of the potential variation is much greater than the tip width itself. The influence on the electrostatic potential causes a change in the distribution of the mobile charges in the semiconductor. The negatively biased tip pushes the electrons away from the semiconductor surface leading to a decrease of the electron concentration underneath
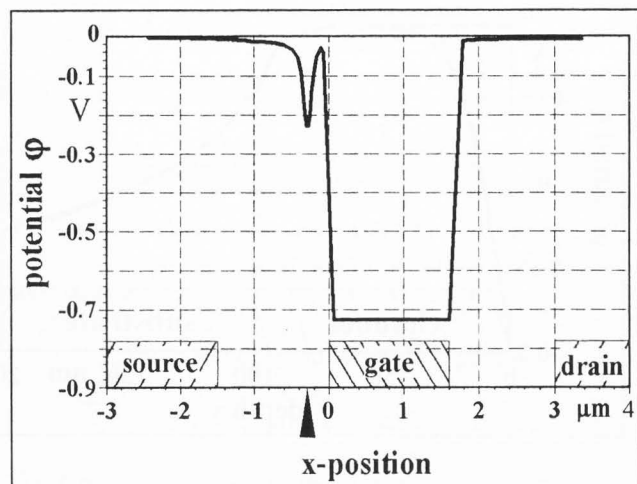
Figure 5. Lateral variation of the electrostatic potential at the semiconductor surface (y = 0 nm) (arrow marks the tip position).
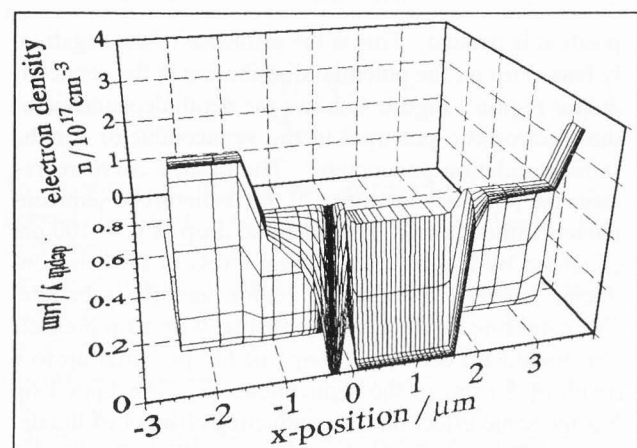

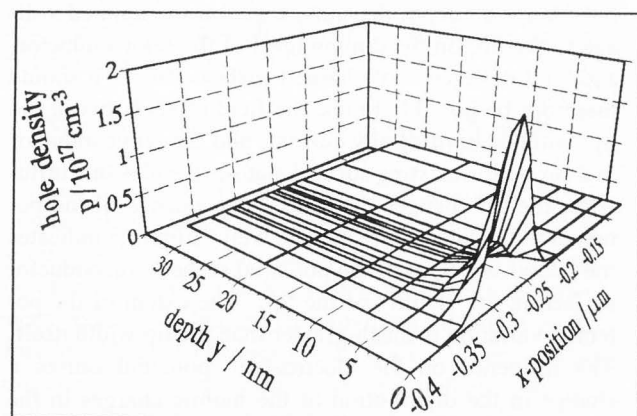**Figure 6.** Spatial distribution of the electron density.

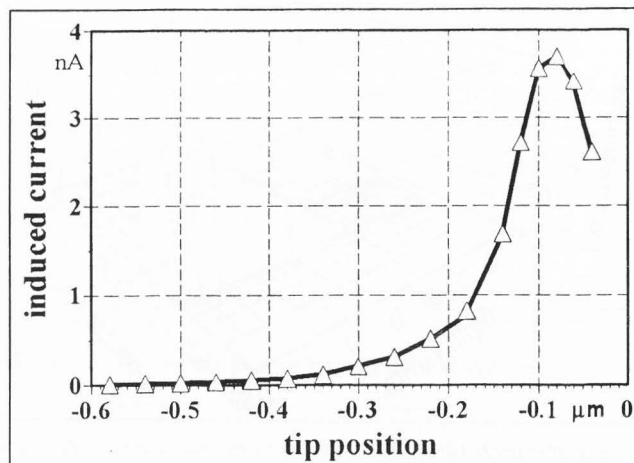**Figure 7.** Spatial distribution of the hole density.

Figure 8. Simulated linescan of the induced current (markers indicate the tip position).

----

the tip (Figure 6), while positively charged holes are attracted by the tip leading to an increased hole concentration underneath the tip (Figure 7). This means that it is possible to produce an enhancement or a depletion region locally limited in the semiconductor underneath the tip, depending on the tip bias.

The numerical simulations cannot only be performed for one specific tip position but also for various positions between the source and the gate contact leading to a simulated linescan. Figure 8 demonstrates the change of the gate current, which is equal to the induced current, depending on the tip position. An exponential increase of the induced current is observed when the tip is approaching the gate contact. For a tip-gate distance below 100 nm, a decrease of the induced current is calculated which can be attributed to a lowering of the potential drop of the Schottky contact in the lateral direction. This simulation result is in accordance with a recent measurement result on a GaAs-MESFET where an exponential increase of the induced current has been reported when a linescan is performed in the manner described above [4].

Conclusions

Based on the semiconductor equations, the influence of a tunneling tip with an applied voltage on electrical parameters like the potential distribution or the charge densities of a GaAs-MESFET was calculated. It was demonstrated that the STM-EBIC measurement technique has an influence on these parameters that cannot be neglected. This influence must be taken into account when this technique is applied to real devices. This unavoidable influence offers the opportunity of using the

tip induced changes as a new measurement technique which is based on the electrostatical interaction between tip and sample, a nano-field-effect microscopy.

Symbol Table

C	density of fixed charges, e.g., charged traps (cm^{-3})
D_p	hole diffusion coefficient ($cm^2\ s^{-1}$)
D_n	electron diffusion coefficient ($cm^2\ s^{-1}$)
e	electronic charge (1.610^{-19} As)
G_{ext}	external carrier generation rate ($cm^{-3}\ s^{-1}$)
GR	carrier generation-recombination rate ($cm^{-3}\ s^{-1}$)
I_{PE}	primary beam current (A)
J_p	minority current density (Acm^{-2})
J_n	majority current density (Acm^{-2})
N_A	acceptor density (cm^{-3})
N_D	donor density (cm^{-3})
n	density of free electrons (cm^{-3})
p	density of free holes (cm^{-3})
$\overline{r}$	position vector (cm)
W_{PE}	primary electron energy (eV)
W_{eh}	mean energy required for e-h-pair generation (eV)
$\langle f(\overline{r})\rangle$	mean spatial distribution of excess carriers (cm^{-3})
ϕ	electrostatical potential (V)
ε_S	semiconductor permittivity
μ_n	electron mobility ($cm^2\ V^{-1}s^{-1}$)
μ_p	hole mobility ($cm^2\ V^{-1}s^{-1}$)

References

1. Ding Z, Wu Z (1993). A comparison of Monte Carlo simulations of electron scattering and X-ray production in solids. J. Phys. D: Appl. Phys. **26**, 507-516.

2. Kaiser WJ, Bell LD, Hecht MH, Davis LC (1993). BEEM and the Characterization of Buried Interfaces. Scanning Tunneling Microscopy and Spectroscopy. VHC Publishers, New York. 251-286.

3. Kazmerski LL (1991). Specific atom imaging, nanoprocessing, and electrical nanoanalysis with scanning tunneling microscopy. J. Vac. Sci. Technol. **B 9**, 1549-1556.

4. Koschinski P, Dworak V, Kaufmann K, Balk LJ (1993). Prospects of an application of a scanning tunneling microscope to electron beam induced current (EBIC) investigations. Proceedings of the DRIP5 Conference, Santander. Institute of Physics Conference Series, Bristol, U.K. Accepted for publication.

5. Ludeke R (1993). Density of states and hot electron effects in ballistic electron emission spectroscopy. J. Vac. Sci. Technol. **A 11**, 768-791.

6. Wenderoth M, Burandt C, Gregor M, Loidl G, Ulbrich RG (1992). Luminescence from gold-passivated gallium arsenide surfaces exited with a scanning tunneling microscope. Solid State Communications **83**, 536-537.

Discussion with Reviewers

D.B. Holt: STM-EBIC appears very attractive, but how difficult or limited is it experimentally? Will you please give some indications of spatial resolutions, sensitivities and signal/noise ratios that your experience suggest should be attainable with commercially available STMs, power supplies, amplifiers, etc.? Also, how difficult and time consuming is it to set up and record measurements?

Authors: The spatial resolution in STM-EBIC is determined by the surface recombination of the minority carriers which leads to a reduced diffusion length in comparison to the bulk value. Therefore, a spatial resolution better than 100 nm should be attainable. The sensitivity of STM-EBIC and the signal/noise ratio are worse compared to that obtainable with conventional SEM-EBIC, because the generation rate is less then that of SEM-EBIC due to the lower energy of the primary electrons, and, besides the noise sources in both methods present, e.g., shot noise and thermal noise one additional STM-EBIC specific source of noise is the statistical fluctuation of the generation rate due to instabilities of the emission current around the adjusted current value if the instrument is working under ambient air condition. This can be avoided by working under rough vacuum conditions. The time to set up measurements is almost equal to that as necessary for conventional EBIC measurements. As for all scanning probe microscopy techniques, it is time consumptive to record measurements due to the limited scan speed because of the cut off frequency of the feed back loop. According to our experience approximately 30 minutes are required to obtain a high quality STM-EBIC micrograph.

D.B. Holt: Is the MINIMOS software available and from whom?
Authors: The original MINIMOS software is available from Prof. Dr. Siegfried Selberherr, Institute for Microelectronics, Technical University Vienna, Gusshausstr. 27-29, A-1040 Wien, Austria. The modified version can be obtained from the authors, but, due to a license agreement, only with the prior permission of Prof. Dr. S. Selberherr.

D.B. Holt: You modelled the hole-electron pair generation as homogenous under the tip, decaying linearly with depth to a maximum penetration of the primary electrons of 20 nm. Is this realistic or merely mathematically simple? What about lateral spreading from the presumable hemispherical probe tip?

Reviewer II: How can the authors justify their assumption that maximum penetration depth of primary electrons is only 20 nm? What is the role of tip asymmetry?

Authors: The determination of the maximum penetration depth from scattering models leads to a penetration depth below 1 nm, which is probably not a correct value. From BEEM measurements, it is known that a fraction of electrons injected into a gold layer of approximately 20 nm thickness can cross this layer. Therefore, we assumed the same value for the penetration depth in GaAs as an initial guess, which must be aligned to further results.

The curvature of the tip and the lateral spreading of the emitted electrons are neglected for convenience (simple rectangular boundary condition). The real tip structure and the current density distribution can be modelled properly incorporating results available from nano field emitter research.

D.B. Holt: You mention that the form of the simulated linescan of Figure 8 resembles a recent experimental result in that both show an exponential increase of the induced current as the gate electrode is approached. Did the experimental result also show the decrease of the induced current for probe-gate distances less than 100 nm predicted by the simulation?

Authors: The experiment did show a decrease of the induced current when the tip is approaching the gate contact. We are not sure if this decrease can be attributed to the potential change calculated in our simulations. Due to the shape of the tip and gate contact used in our experiment, we cannot exclude completely that there might be a direct contact between the upper part of the tip and gate contact when the tip is approaching the gate contact leading to a rapid decrease of the induced current.

Reviewer II: Why does the peak induced current (Fig. 8) not coincide with the zero tip position (peak current occurs at 0.75 μm away from the tip position)?

Authors: Due to the negatively biased tip, a decrease of the lateral potential gradient occurs leading to a reduced current density in direction to the gate of the minority carriers. This results in a reduced induced current.

Reviewer II: From Figure 4, you deduce that "The effect of biased tip causes a change in potential up to a depth of 50 nm in a semiconductor". Please explain the conditions. Also, what is the role of surface charges?

Authors: The conditions in our simulations are as follows: doping level of the active layer n = $3.0 \cdot 10^{17}$ cm^{-3}, tip voltage -10 V, and distance tip-surface 40 nm. The change in depth of the potential depends on the doping level of the semiconductor, on the tip bias, and on the surface charges present. Surface charges are not taken into account in our simulations. These charges affect only poisson's equation, therefore an additional term, which is unequal to zero only at the semiconductor surface, has to be added to this equation. However, the surface charges present influence the potential distribution under the semiconductor surface and therefore the induced current, too.